INTERNATIONAL SOCIETY FOR SOIL MECHANICS AND GEOTECHNICAL ENGINEERING

A comparison between static and dynamic load tests of Tapered steel jacking piles in Baskarp sand

Junyu Zhou[1], *Yimo* Wu[1], *Lars Bo* Ibsen[1], and *Amin* Barari[1,2#]

[1]*Aalborg University, Department of the Built Environment, Thomas Manns Vej 23, 9220 Aalborg Ø, Denmark*
[2]*RMIT University, School of Engineering, Melbourne VIC 3000, Australia*
[#]*Corresponding author: amin.barari@rmit.edu.au*

ABSTRACT

In this study, four full scale static compression tests were performed on a tapered steel jacking pile with diameters 76 mm and 89 mm in both dry and saturated soil conditions. Each test consists of multiple sub-tests with respect to determination of in-situ Baskarp Sand No.15 conditions and bearing capacities of the piles. Further, a finite element methodology has been developed to predict the load-displacement response of tapered piles installed in sand, incorporating the effects of jacking installation. The methodology is based on the identification of the failure mechanism and shear strain formation at failure around the pile as well as adoption of soil-soil interface elements. The nonlinear soil model parameters for a fully wished-in-place (fully-WIP) condition were obtained through piezocone penetration tests where various methods were applied to obtain the relative density, among which those providing best fit according to Jamiolokowski et al., (2003) were selected for further assessment. Finally, the hammer tests were performed from which the dynamic bearing capacities and the relation between static and dynamic bearing capacities were obtained.

Keywords: Tapered piles; static bearing capacity; dynamic; finite element; installation.

1. Introduction

According to the Alwalan and El Naggar (2020) screw pile is an efficient foundation solution for many different engineering projects where high compressive, and uplift resistance to static and dynamic loads is a requisite. Screw piles differ from traditional piles as they consist of helices fixed to the shaft at a specific spacing. The screw piles have a pointy toe to allow for better installation into the ground. However, the soil-pile interface behaviour may be largely influenced by the mutual interplay of pile shaft and helices and can be relatively complicated.

To provide an improved understanding of the behaviour of screw piles in disturbed soil and isolate the individual contribution of pile components, laboratory tests along with FE predictions with full scale tapered jacking piles were presented. The designated tapered pile has the similar dimensions and material properties as the screw piles, with the exception of not having threads. The tapered piles can be seen in Figure 1.

Tapered piles, including natural timber piles and those manufactured of steel or concrete, are widely used in practice (Horvath and Trochalides 2004). The existing literature has emphasized the tapered piles possess improved static axial capacity compared with conventional piles while developing analytical models for predicting the static capacity of tapered piles (El Naggar and Wei 1999; Khan et al., 2008; Kodikara and Moore 1993; Liu et al., 2012).

In the current study, two different pile geometries were evaluated, see Table 1; the main objective of this paper is to adopt a FE methodology to predict the compressive performance of jacking tapered piles which accounts for capacity, stiffness and installation process as well as to determine a correlation between static and dynamic bearing capacity in compression for steel tapered piles installed by jacking in sand with varying relative densities. The piles are installed by a static compression load test that includes an unloading/reloading step. The cone penetration tests (CPT) and piezocone penetration tests (CPTu) are performed to capture the soil state prior to and following installation of the piles. Finally, a hammer test is performed in order to facilitate the determination of the bearing capacity, i.e., the relationship between static and dynamic bearing capacity.

Table 1. Dimension of Tapered piles.

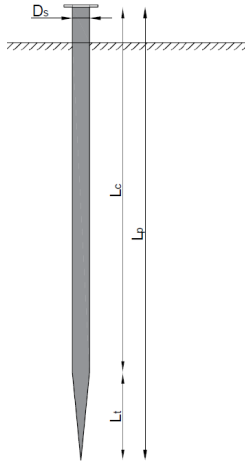| Pile tests	Pile diameter d_s (mm)	Pile length L_p (mm)	Tapered length L_t (mm)	Cylindrical length L_c (mm)
P76	76	2070	400	1670
P89	89	2070	400	1670

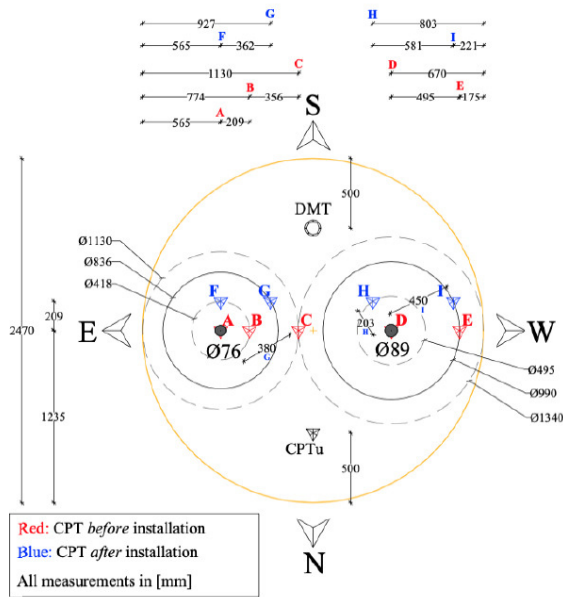**Figure 1**. Sketch of a tapered steel jacking pile

Figure 2. An overview of the CPT tests performed for P76 and P89 piles.

2. Test description

In total, nine laboratory tests are conducted at Aalborg University (AAU) Offshore Geotechnics Laboratory (Barari and Ibsen 2017, Ibsen et al. 2015, Barari and Ibsen 2014) in a steel tank called yellow tank (Rodriguez et al. 2022), where test 2, 4, 6 and 8 were carried out in dry sand condition, and the left tests were in saturated condition. This circular tank is 2470 mm in diameter and 3520 mm in depth, which filled with Baskarp sand No.15. The Baskarp sand has been widely tested and its properties are detailed in Barari et al. (2021) and Ibsen et al. (2009).

Each set of experiments includes the installation of two different tapered piles with the diameters 76 mm and 89 mm (called P76 and P89 henceforth) with lengths of 2.07 m in the tank. There are two different types of actuators: Actuator 1 which has a maximum force of 60 kN and a range of position from-750 mm to 750 mm meaning 1.5 m motion. Actuator 2 has a maximum force of 250 kN and a range of position from-300 mm to 300 mm meaning 0.6 m motion. These actuators are used for

several tests besides the ones directly to the pile, this includes CPT, CPTu, DMT, sample tube, and the load tests performed on the piles. The positions are chosen with inspiration from ISO 22741-1 (2018) which requires free distance from tested pile of 2.5 to 5 times the diameter. The piles are installed by a static compression load test to a depth of around 1.8 m that includes an unloading/reloading step. For each test, two types of cone penetration tests CPT and CPTu are designated. Here, CPT makes it possible to compare the soil state before and after the pile installation. Therefore, the CPTs are placed as shown in Figure 2 (i.e, 5 CPTs prior to and 4 following installation). Hence the influence of the rupture zone can be observed as the diameter multiplied with the factors 2.5 and 5 based on the standard ISO 22741-1 (2018). Furthermore, a hammer test is performed in order to facilitate the determination of the bearing capacity while obtaining an empirical relationship between static and dynamic bearing capacity; for this, an empirical procedure as detailed in "Den Danske Rammeformel (DDR)" (Ovesen et al. 2012) is utilised. Note the results of CPT tests prior to and following installation are exclusively used to examine how the installation effects influence the relative densities of the soil deposit. Two tests out of nine (tests 4 and 5) were selected for providing numerical predictions and calibration with HSsmall and UBC3DPLM soil models (Brinkgereve et al. 2018; Galavi et al. 2013). The sand's relative densities of interest are 73.4% and 53% belonging to dense and medium-dense soil conditions, respectively.

2.1. Determination of soil parameters

In this paper for the sake of wished-in-place simulation, the soil parameters are directly estimated based on the empirical equations presented as a function of the relative density D_r as presented in Ibsen et al. (2009); based on a collation of triaxial and other test data from Baskarp sand (Table 2). The relative density was determined using CPTu test data prior to the installation. Figure 3 demonstrates the estimate of relative density prior to installation for test 4. Among various approaches examined here, Jamiolkowski (2003) is the method that gives the loosest soil state compared to the other methods, after disregarding the AAU, $D_r = 5.14 \left(\frac{\sigma'_{v0}}{q_c^{0.75}} \right)^{-0.42}$ (i.e., q_c is the cone resistance) and Schmertmann (1978) methods and thereby it is chosen, principally due to a conservative estimate of D_r. The empirical relationship between the effective vertical stress, cone resistance and relative density is expressed in Eq. (1):

$$D_r = \frac{1}{C_2} ln \left[\left(\frac{q_c}{P_a} \right) \bigg/ C_0 \left(\frac{\sigma'_{v0}(\frac{1+2K_0}{3})}{P_a} \right)^{C_1} \right] \quad (1)$$

where C_0, C_1, and C_2 are soil constants, P_a is atmospheric pressure, σ'_{v0} is effective overburden pressure and K_0 is coefficient of lateral earth pressure at rest.
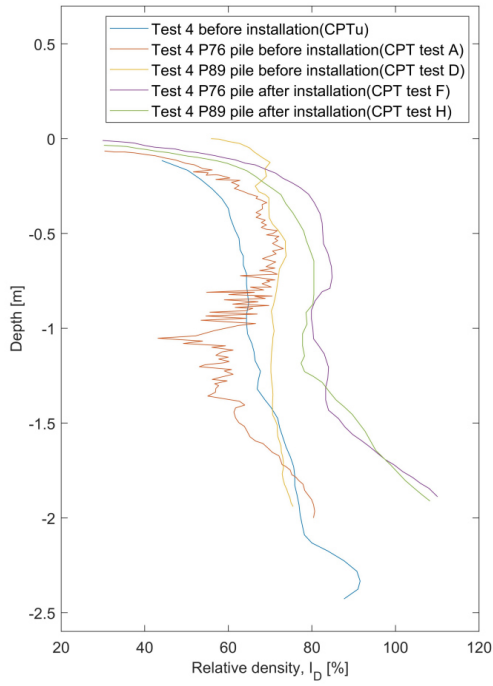
Figure 3. D_r determined prior to and following installation in test 4

Table 2. HSsmall model parameters for fully-WIP models in Baskarp sand (Ibsen et al. 2009) and Semi-WIP

Soil parameters	Unit	Equation (WIP)	Test 4 (Semi-WIP)
Peak friction angle, ϕ'_p	[°]	$0.11D_r + 32.3$	36.4
Dilatancy angle, ψ	[°]	$0.195D_r + 14.9\sigma'^{-0.0976}_3 \cdot 9.95$	10.80
Effective apparent cohesion, c'	[kPa]	$0.032D_r + 3.52$	1.80
Oedometer stiffness, E^{ref}_{oed}	[kPa]	...	3.17×10^3
Reference secant stiffness modulus, E^{ref}_{50}	[kPa]	$0.6322D_r^{2.507} + 10920$	3.95×10^3
Reference unloading/reloading stiffness modulus, E^{ref}_{ur}	[kPa]	…	28.5×10^3
Threshold shear strain, $\gamma_{0.7}$	[-]	…	1.1×10^{-3}
Poisson's ratio, v'	[-]	$\dfrac{1 - sin(\varphi')}{2 - sin(\varphi')}$	0.2
Material parameter, m	[-]	…	1
Earth pressure at rest, K_0	[-]	…	0.406

Table 3. Calibrated UBC3D-PLM model parameters with soil-soil interface elements

Parameters	Unit	Value (Test 5)
Dry unit weight, γ_{unsat}	$[kN/m^3]$	14.5
Saturated unit weight, γ_{sat}	$[kN/m^3]$	16.5
Initial void ratio, e_{int}	[-]	0.694
Elastic bulk modulus factor, k^{*e}_B	[-]	28.5
Elastic shear modulus factor, k^{*e}_G	[-]	45
Plastic shear modulus factor, k^{*p}_G	[-]	12
Rate of stress-dependency of elastic bulk modulus, me	[-]	0.50
Rate of stress-dependency of elastic shear modulus, ne	[-]	0.50
Rate of stress-dependency of plastic shear modulus, np	$[kN/m^2]$	0.40
Constant volume friction angle, ϕ_{cv}	[°]	21.50

2.2. Finite Element simulations of model tests

The model tests were computationally modelled using PLAXIS 3D Finite Element software code. The tapered piles were modelled by neglecting the cone shape in level across bottom of pile. Hence, an idealized geometry, is produced by simplifying the tapered pile into cylinder with a flat bottom. Each pile was modelled using a volume cluster with linearly elastic non-material behaviour with unit weight of steel $\gamma_{steel} = 78.5 \frac{kN}{m^3}$, Poisson's ratio= 0.3 and Young's modulus E=210 GPa. The FE mesh discretization used is shown in Figure 4. The soil was subdivided into zones to subsequently allow finer mesh size close to the piles. Initially the model domain was defined such that extending 3D in length and 3L in depth, where L and D are the diameter and embedded length of the tapered pile, respectively. Roller supports were assigned to the side boundaries, where the horizontal movement is restricted, and a free deformation boundary is assigned to the top of the model.

The tapered pile model was formed by simplifying into cylindrical shape with a flat base. Initial stresses were generated by means of K_0 procedure.
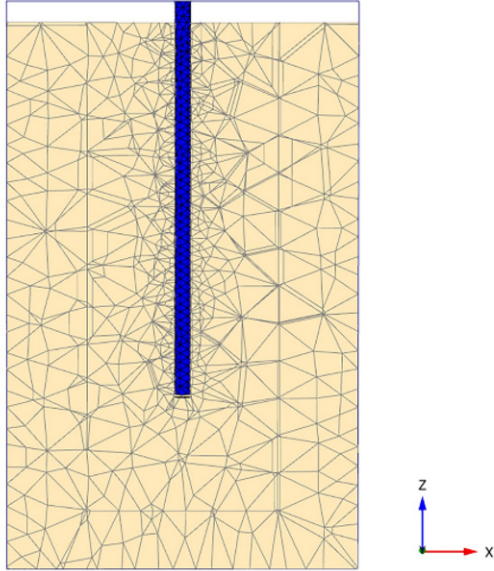
Figure 4. The Finite Element mesh discretization

2.3. Modelling methodology

To facilitate comparisons between with and without installation effects as depicted in Figure 3 by lumping into D_r change, three different types of models are implemented into FE software code, which consist of fully wished-in-place (fully- WIP), semi-WIP and fully-influenced models incorporating installation effects. They are described as follows:

(a) Fully wished in place (Fully-WIP)

In the first stage analysis, the fully-WIPmodels are simulated where installation effects of the piles are not taken into consideration. Initially soil parameters determined based on the CPT tests prior to installation are directly input into the FE model, and the embedded length of the tapered pile is set equal to the recorded pile depth at the end of the installation phase in experiments. Afterwards, a vertical load corresponding to the maximum load in unloading-reloading test is applied to the pile.

(b) Semi-wished in place (Semi-WIP)

In the second stage, an enhanced numerical model was developed by imposing a modified stress field distribution around the pile shaft accounting for static compression load gradually increasing to the final load reported from the installation rig.

(c) Fully-influenced model

Finally, to completely incorporate the installation effect in numerical models, the calibrated soil parameters from the second stage (Tables 2 and 3) and the relative densities determined from post-installation CPT tests are required. In the simulation of the fully-influenced model, it is also necessary to introduce soil-soil interface elements that account for softening behaviour in saturated sand while pre-loading the soil body to ensure that the installation effect is taken into consideration, in which a compression load with the same magnitude of final loads in the unloading-reloading phase in accordance with the experiments is applied.

3.   Results and Discussions

3.1. FE predictions against static load tests

The load-displacement curves for the fully-WIP model and the experimental data are demonstrated in Figure 5, where stiffer measured response is observed. The difference between these two load-displacement curves is expected to be resulted from lack of pre-stressing mechanism in foundation soil occurring due to jacking installation. To explicitly address this, additional study was carried out using semi-WIP model. From Figure 6, it is obvious that after adopting a Semi-WIP model provides a reasonably good calibration basis, and this support its relevance for jacking tapered piles.
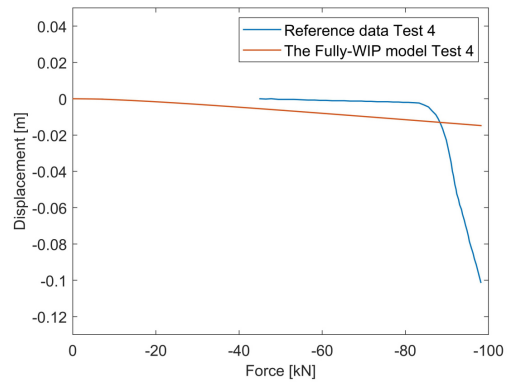

Figure 5. Load-displacement behaviour from the experimental results and the fully-WIP model (P76: Test 4)
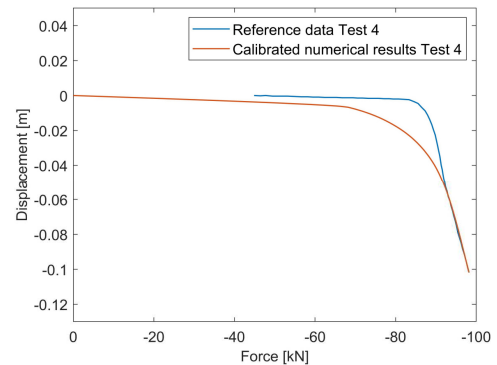

Figure 6. Load displacement behaviour of the Semi-WIP model for P76: Test 4 using the HS-small model and the experiment results.

Nevertheless, after various attempts, the semi-WIP model for tests in saturated soil conditions (P76-5 and P89-5) was found elusive when compared with the experimental observations. Authors acknowledge that this can be attributed to softening behaviour in the vicinity of pile shaft due to installation disturbance in saturated sand which results in the soil deposit losing its strength. Consequently, a slightly weaker response than the numerical results is seen. Further simulations are carried out with the UBC3D-PLM model incorporating the soil-soil interface elements.

During the loading process, only the vertical compression load is applied to the pile. In this case, it is expected that the axial strain, ε_1, in a limited zone in the upper part of the soil sample will become larger which may lead to a reduction of the soil strength. As the soil sample analysed in Test 5 (saturated condition) is the

medium-dense sand, it is likely that the soil softening will happen after the soil reaches the peak value.

Here, the fully-WIP model is initially loaded by a vertical compression load, of which the magnitude is equal to the recorded final installation load from the experiments. Subsequently, the vertical load is reduced to zero. It is assumed that the soil sample reaches the failure state at the displacement of 0.2D.

The distribution of vertical principal strain, ε_1, over the embedded depth of the pile is illustrated below in Figure 7. It should be noted that this figure only presents the result of the last step in the loading phase for the fully-WIP model. On the basis of the distribution of the principal vertical strain, the depth of the strength reduction zone is conservatively designated as 0.17 m (Figure 8).

The load-displacement curve for test P76-5 using UBC3D-PLM with soil-soil interface elements is shown in Fig. 9. Compared with the numerical results with soil-structure interface, the strength level has a satisfactory reduction.
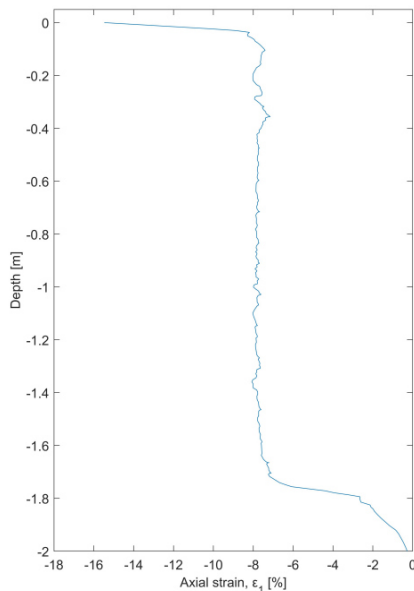

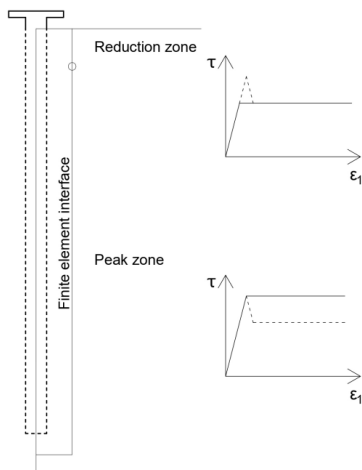**Figure 7.** The strain distribution along the pile shaft for test 5

Figure 8. Principal strain distribution along the distance in Y-direction
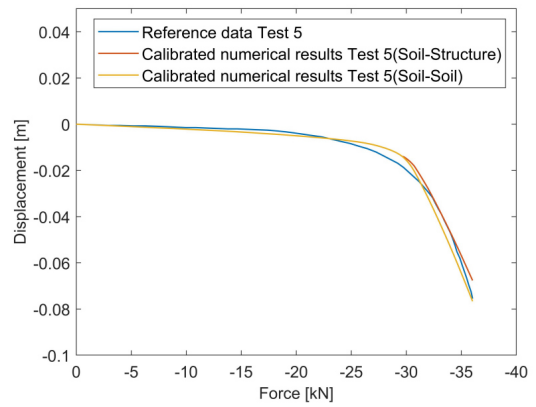

Figure 9. Load-displacement curves of the calibrated model using UBC3D-PLM model (soil-soil interface) and the experimental data for test 5

3.2. Determination of dynamic bearing capacity

Although it is widely accepted to conduct a static load test to determine the bearing capacity, this process can be of high computational costs and time consuming, particularly when the piles are considered as large capacity. Alternatively, high strain dynamic load test has been successfully applied to piles.

Nowadays, there is a demand for performing dynamic load test on piles in sand.

Therefore, the relation between the static and dynamic bearing capacities i.e., J-factors are of interest. The hammer test was carried out on both piles, by a hammer from increasing drop heights of 218, 418, 618, 818 and 1018 mm. The hammer consists of a sleigh with multiple attached steel plates weighting 19.31 kg on average and the sleigh itself weighs 18.55 kg. The sleighs is controlled by the rod in which the holes are placed for every 200 mm allowing for the designated drop heights (Figure 10).

Figure 10. Hammer test configuration

The mass of the hammer G, and thus the number of steel plates to apply is controlled by the maximum static force, R_s, required to install the pile to a depth of approximately 1.9 m (i.e., after unload/reload test). The mass is chosen as suggested by DDR approach with a drop heigh, h of 618 mm and a settlement, s of 10% of the pile diameter. The efficiency factor, η, is assumed to be 1.

$$G = \frac{R_s s + 0.5 s_0}{\eta h_{drop}} \qquad (2)$$

The elastic settlement, s_0, is calculated from the maximum static force and pile diameters: length, l_p, cross sectional area, A, and Young's modulus for steel, E_{steel}:

$$s_0 = \frac{R_s l_p}{A \cdot E_{steel}} \qquad (3)$$

Thereby the number of plates is found from:

$$n_{plates} = \frac{G - 18.55}{19.33} \qquad (4)$$

During the tests, the settlement of the pile is measured with a 1 mm accuracy for each hammer stroke, and it is monitored that the settlement is around 10% of the pile diameter when the drop height is 618 mm. After the hammer test, an additional static installation of 100 mm is performed.

The potential energy from a hammer stroke is used to exceed the piles resistance against penetration and thereby gives the pile a remaining settlement. For this, DDR is applied (Ovesen et al., 2012):

$$\eta h_{drop} G = R_s s + \frac{1}{2} R s_0 \qquad (5)$$

A settlement of 10% of the pile diameter is expected for a drop height of 618 mm, and therefore these results are presented in this section.

As there sometimes is a big difference between the applied and theoretical weight, a ratio between those two is found by the following:

$$R_{mass} = \frac{\text{Applied mass}}{\text{Theoretical mass}} \qquad (6)$$

The ideal ratio between the applied and theoretical mass is 1, but as the theoretical mass is not sufficient for a theoretically expected settlement of 0.1D corresponding to 10% of the pile diameters for a drop height of 618 mm, a bigger mass was sometimes applied. The ratio between obtained and theoretical settlement is found by the following:

$$R_{settlement} = \frac{\text{Obtained settlement}}{\text{Theoretical settlement}} \qquad (7)$$

The ratios for mass and settlement along with the maximum static load are presented in table 4 for pile model tests P76 and P89. The dynamic bearing capacity, R_d, is obtained from Eq. 8 which is derived from Eq. 5:

$$R_d = \frac{\eta h_{drop} G}{s + \frac{1}{2} s_0} \qquad (8)$$

The static bearing capacity, R_s, is obtained from static compression load tests. The results are presented along with the ratios between the dynamic and static bearing capacities in Table 4. The ratios are found by the following:

$$Ratio = \frac{R_d}{R_s} \qquad (9)$$

Table 4. Hammer test data for P76 and P89 for 618 mm drop height

Test no.	P76-4	P76-5	P89-4	P89-5
Maximum static load [kN]	98	37	137	53
Theoretical mass [kg]	133	52	206	82
Applied mass [kg]	115	57	192	76
Settlement [mm]	11	8	13	8
Static bearing capacity [kN]	89	35	123.40	46
Dynamic bearing capacity [kN]	64.5	40	83.80	53
Ratio	0.7	1.1	0.68	1.1

4. Conclusions

According to the full-scale tests characteristics conducted on Tapered steel jacking piles two tests in dry and saturated Baskarp sand conditions were selected for further investigation through FE modelling. To explicitly address the jacking installation effect, the Tapered model piles are simulated with a three-stages FE modelling approach, where fully-WIP models, Semi-WIP and fully-influenced models were developed.

The comparison with the measured data reveals a large scatter may exist when the in-situ HSsmall soil model parameters prior to installation are directly used in FE computation. Hence, an enhanced modelling procedure was suggested requiring a calibration of soil parameters. Furthermore, UBC3D-PLM model with the soil-soil interface was finally adopted for the calibration of selected test in saturated conditions. Finally, dynamic pile testing using a hammer was performed to obtain a simple yet robust correlation between static and dynamic load-bearing capacities of tapered piles for the sake of preliminary design.

References

Alwalan, M. F, and El Naggar, M. H. 2020. "Finite element analysis of helical piles subjected to axial impact loading", *Computers and Geotechnics*, 123, 103597.

Baldi, G., Bellotti, R., Ghionna, V., Jamiolkowski, M, and Pasqualini, E. 1986. "Interpretation of CPT's and CPTU's. 2nd Part: Drained Penetration." *Proceeding 4th International on Field Instrumentation and in-Situ Measurements,* Singapore, November 1986, 143-156.

Alwalan, M. F, and El Naggar, M. H. 2020. "Finite element analysis of helical piles subjected to axial impact loading", *Computers and Geotechnics*, 123, 103597.

Barari, A, and Ibsen, L.B. 2014. "Vertical capacity of bucket foundations in undrained soil." *Journal of Civil Engineering and Management*, 20(3): 360-371.

Barari, A, and Ibsen, L.B. 2017. "Insight into the lateral response of offshore shallow foundations." *Ocean Engineering*, 144: 203-210.

Barari, A., Ghaseminejad, V, and Ibsen, L.B. 2021. "Failure envelopes for combined loading of skirted foundations in layered deposits." *Journal of Waterway, Port, Coastal, and Ocean Engineering*, 147 (4), 04021008

Brinkgreve, R.B.J., Engin, E. and Swolfs, W.M. 2013 *Plaxis 3D, General Information Manual.*

El Naggar, M. H, and Wei, J.Q. 1999. "Axial capacity of tapered piles established from model tests." *Can. Geotech. J.* 36 (6): 1185–1194.

Galavi, V., Petalas, A, and Brinkgreve, R.B.(2013). "Finite element modleing of siemic liquefaction in soils." *Geotechnical Engineering*, 44(3), 55-64.

Horvath, J.S, and T. Trochalides. 2004. "A half century of tapered pile usage at the John F. Kennedy international airport." In *Proc., 5th Int. Conf. on Case Histories in Geotechnical Engineering*, Rolla, MO: Univ. of Missouri.

Ibsen, L.B., Barari, A, and Larsen, K.A. 2015. "Embedment effects on vertical bearing capacity of offshore bucket foundations." *Journal of Waterway, Port, Coastal, and Ocean Engineering*, 141(6), 06015005.

Ibsen, L.B., Hanson, M., Hjort, T, and Thaarup, M. 2009. "*MC-Parameter Calibration of Baskarp Sand No.15*." Aalborg University, Department of Civil Engineering, ISSB 1091-726X, DCE Technical Report No.62.

ISO 22477-4. 2018. "*Geotechnical investigation and testing-testing of geotechnical structures-part 4: testing of piles: dynamic load testing*." Edition 1, ISO/TC 182 Geotechnics, 52 pages.

Jamiolkowski, M., Manassero, M., Presti, D.C. 2003. "Evaluation of relative density and shear strength of sands from CPT and DMT." *Geotechnical Special Publication*, DOI: 10.1061/40659(2003)7.

Jamiolkowski, M., Baldi, G., Bellotti, R., Ghionna, V, and Pasqualini, E. 1985. "Penetration resistance and liquefaction of sands." XI ICSMFE, San Francisco, 4: 1891-1896.

Kodikara, J. K, and Moore, I. D. 1993. "Axial response of tapered piles in cohesive frictional ground." *J. Geotech. Eng.*, 119 (4): 675–693. https://doi.org/10.1061/(ASCE)0733-9410(1993)119:4(675)

Khan, M. K., M. H. El Naggar, and M. Elkasabgy. 2008. "Compression testing and analysis of drilled concrete tapered piles in cohesive frictional soil." *Can. Geotech. J.*, 45 (3): 377–392. https://doi.org/10 .1139/T07-107.

Liu, J., He, J., Wu, Y.P, and Yang, Q. G. 2012. "Load transfer behaviour of a tapered rigid pile." *Géotechnique*, 62 (7), 649–652. https://doi.org/10 .1680/geot.11.T.001

Ovesen, N. K., Fuglsang, L. D., Bagge, G., Krogsbøll, A., Sorensen, C.S., Hansen, B., Bødker, K., Thøgersen, L., Galsgaard, J., Augustesen, A.H. 2012. "*Lærebog i Geoteknik.*" volume 2 edn, Polyteknisk Boghandel og Forlag, 415 pages.

Rodriguez, F.M.G., Ibsen, L.B., Koteras, A.K, and Barari, A. 2022. "Investigation of the penetration resistance coefficients for the CPT-based method for suction bucket foundation installation in sand." *International Journal of Geomechanics*, 22(6): 04022063.

Schmertmann J.H. 1978. "*Guidelines for cone penetration test performance and design*." US Dept. of Transportation, FHWA, R.78-209. Washington D.C.